

# PanSR: An Object-Centric Mask Transformer for Panoptic Segmentation

Lojze Žust, Matej Kristan  
 University of Ljubljana  
 Večna pot 113, 1000 Ljubljana, Slovenia  
 {lojze.zust, matej.kristan}@fri.uni-lj.si

## Abstract

*Panoptic segmentation is a fundamental task in computer vision and a crucial component for perception in autonomous vehicles. Recent mask-transformer-based methods achieve impressive performance on standard benchmarks but face significant challenges with small objects, crowded scenes and scenes exhibiting a wide range of object scales. We identify several fundamental shortcomings of the current approaches: (i) the query proposal generation process is biased towards larger objects, resulting in missed smaller objects, (ii) initially well-localized queries may drift to other objects, resulting in missed detections, (iii) spatially well-separated instances may be merged into a single mask causing inconsistent and false scene interpretations. To address these issues, we rethink the individual components of the network and its supervision, and propose a novel method for panoptic segmentation PanSR. PanSR effectively mitigates instance merging, enhances small-object detection and increases performance in crowded scenes, delivering a notable +3.4 PQ improvement over state-of-the-art on the challenging LaRS benchmark, while reaching state-of-the-art performance on Cityscapes. The code and models will be publicly available on [GitHub](#).*

## 1. Introduction

Panoptic segmentation is a fundamental scene understanding problem that jointly addresses semantic segmentation and object detection/instance segmentation tasks. Recent advances have led to the emergence of mask transformer architectures [4, 5, 13] with the potential to handle these tasks in a unified architecture.

Mask transformers [5, 9, 13] perform panoptic segmentation through a set of learnable queries, each encoding an individual mask instance. These queries are gradually refined via cross-attention with multi-scale image features in the transformer decoder. From the final refined queries, object label, mask and optionally a bounding box are predicted. During training, bipartite matching

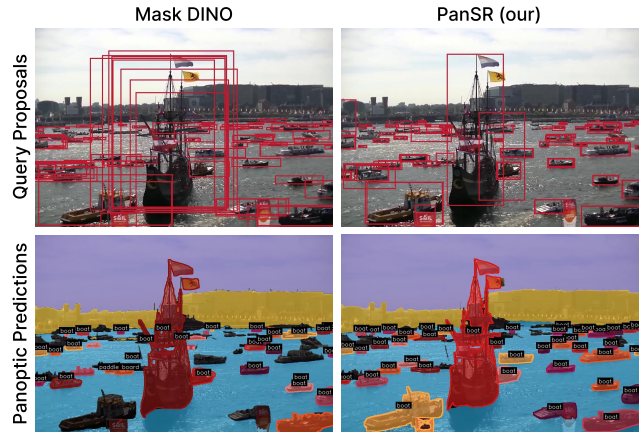


Figure 1. Recent transformer-based methods for panoptic segmentation rely on a simple query proposal approach (top left) and struggle with instance separation (bottom left). PanSR presents object-centric query proposals (top right) and reworks the mask decoding process for thing classes, leading to significant improvements in instance segmentation (bottom right).

is used for optimal matching between learnable queries and ground-truth instances. This leads to excellent performance on general panoptic benchmarks such as COCO [1] and ADE20k [22], as well as scene parsing in autonomous vehicles Cityscapes [6]. However, several shortcomings were exposed on the recent maritime scene understanding benchmark for autonomous boats LaRS [24]. A crucial difference from the related autonomous cars scenes is that the visibility range is substantially larger in maritime scenes. This leads to scenes with a much higher diversity of observed objects' sizes.

Recent advances in the detection capabilities of mask transformers, replacing learnable queries with query selection (*i.e.* proposals) mechanisms [13, 21], improve the robustness of models to different object scales. However, we observe that the simple top-k response selection process used in these methods is biased towards large objects due to their relatively larger pixel count, often leading to missed detections of small objects in the same scene (see Figure 1).

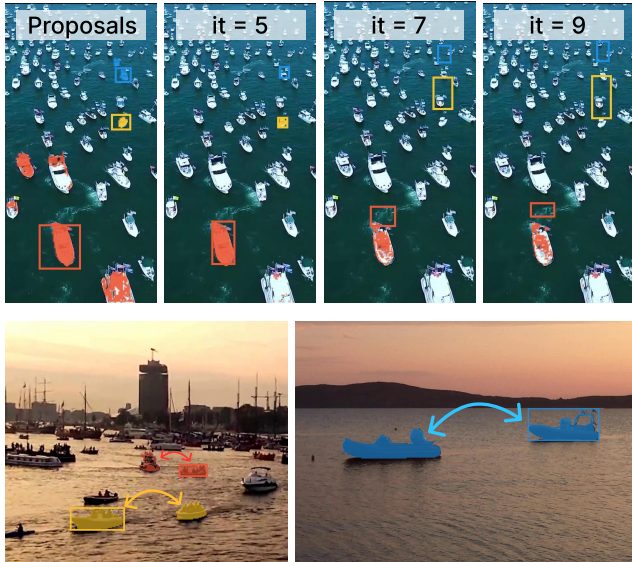


Figure 2. Failure cases of mask transformers: well-initialized queries drift away from original objects during decoder iterations (top), and well-separated objects become merged by predicted segmentation masks (bottom). Colors indicate instance labels.

Another issue is *query drift*. The bipartite matching used in training encourages the decoding of matched queries towards the corresponding ground-truth, while pushing the unmatched queries away. However, in case of several proposals generated on the same object, one query will be favored to match the object, while the others tend to be pushed toward other objects. This leads to unpredictable behavior at test-time, where well-generated initial queries drift away from the object during the decoding, even in the absence of alternative queries for the same object (see Figure 2).

Lastly, instance masks are computed by correlating the decoded query with high-resolution image features. This requires learning of strong features to distinguish instance of visually similar objects in feature space. In practice, however, the resulting masks may merge several spatially well-separated instances (Figure 2), even when bounding boxes are correctly localized. This is especially common in crowded scenes.

To address the aforementioned issues, we propose PanSR, a new scale-robust mask transformer for panoptic segmentation, which is our primary contribution. The method introduces several design novelties: **(i)** To capture objects at all scales, we introduce an object-centric proposal module (OCP), which shifts proposal extraction from pixel level to object level and improves performance on small objects. **(ii)** To alleviate query drift, we introduce a new proposal-aware matching scheme, which prevents matching of proposals to incorrect ground-truth instances, and allows multiple proposals to match to a single ground-truth

instance. This removes the competition between the proposals of the same object and instead encourages them to decode alternative predictions for the same object. **(iii)** To address the problem of instance merging, we introduce object-centric mask prediction, which constrains the mask prediction by the predicted bounding boxes. This removes the requirement of learning strong global instance separation features and frees up the network capacity for other capabilities. **(iv)** Finally, to improve robustness to variance in the proposal extraction process, we introduce a set of mask-conditioned queries during training, by sampling queries from random locations in object regions.

PanSR outperforms all state-of-the-art methods by a large margin (+3.4% PQ) on the recent challenging LaRS [24] benchmark and performs on par with the best methods on Cityscapes [6] (67.3 PQ). Quantitative and qualitative analysis reveals superior performance, primarily on small objects, in dense scenes, and in scenes with many similar objects.

## 2. Related Work

Panoptic segmentation emerged as a natural merging of semantic segmentation and instance segmentation tasks. This is also reflected in the early methods [3, 10, 11, 18], which feature a two-branch (semantic and instance) approach with a post-processing fusion of the two outputs.

However, most recent approaches follow a mask-transformer architecture [4, 5, 16], which reformulates all segmentation tasks (semantic, instance, panoptic) as mask prediction and classification. Inspired by detection transformers [2], they use a set of instance queries, where each query is decoded into a single instance mask and corresponding class label.

Recent efforts focus on bridging the gap between panoptic segmentation and detection, by including a bounding box regression head and integrating key insights from recent improvements in detection transformers such as replacing learnable queries with query selection [20, 23] and de-noising queries [12, 14, 20] to mask-transformers [13]. While this leads to much better detection performance, the process selects queries at top  $k$  per-pixel score prediction locations, which inherently favors larger objects. Furthermore, with the introduction of these changes, other design choices of mask transformers, which are optimized for learnable queries, have not been reconsidered.

The inherent differences between thing and stuff classes have only been explored recently. A more natural separation into stuff and thing queries were proposed [21], where learnable queries are used for semantic stuff classes, and query selection is used for thing class instances. We adopt a similar strategy in PanSR.

Several recent approaches integrate vision-language models in an open-vocabulary [19, 21] or a multi-task [9]

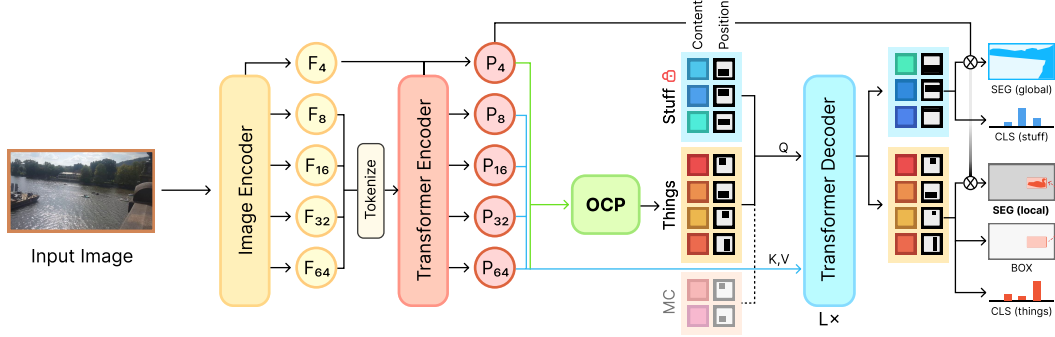


Figure 3. Architecture of PanSR. The backbone features are processed by a transformer encoder into a feature pyramid. Object-Centric Proposal extractor (OCP) is used to obtain thing queries. A transformer decoder refines the instance queries. The predicted masks of thing classes are limited by their predicted bounding boxes. Mask-conditioned queries (MC) ensure robustness to noise in proposal extraction.

strategy, removing the constraint of fixed class-sets or tasks. These approaches achieve excellent results by enabling training on multiple datasets or tasks without need for explicit class alignment, but do not address the fundamental issues of mask-transformers tackled in this paper. In this respect, the method we propose is complementary to the vision-language model integration.

### 3. PanSR

At a high level, our method (see Figure 3) follows a mask-transformer architecture [5, 13]. The input image  $\mathbf{I} \in \mathbb{R}^{H \times W \times 3}$  is encoded by image encoder into features  $\mathbf{F}_s$ , where  $s \in \{4, 8, 16, 32, 64\}$  denotes the stride of the feature maps. The features are further refined by a transformer encoder self-attending the features across scales and building a multi-scale feature pyramid  $\mathbf{P}_s$ .

A set of  $N$  instance queries are used to represent the potential object instances. They are composed of content ( $\mathbf{Q}_f \in \mathbb{R}^{N \times 256}$ ) and positional (*i.e.* bounding-box,  $\mathbf{Q}_{\text{box}} \in \mathbb{R}^{N \times 4}$ ) queries. Due to the unique characteristics of stuff and thing classes, we further split the queries into  $N_{\text{st}}$  stuff and  $N_{\text{th}}$  thing queries and employ slightly different strategies for their decoding and supervision (see Section 3.1).

Content and positional queries are iteratively refined in several transformer decoder layers  $\mathcal{D}_t$ , by attending them with the multi-scale image features, *i.e.*

$$\mathbf{Q}_f^{t+1}, \mathbf{Q}_{\text{box}}^{t+1} = \mathcal{D}_t(\mathbf{Q}_f^t, \mathbf{Q}_{\text{box}}^t, \mathbf{P}_s), \quad (1)$$

where  $t \in [1..L]$  denotes the iteration number. Finally, mask, bounding box and class predictions for each query are obtained via the prediction heads

$$\mathbf{M}_t = \mathcal{M}(\mathbf{P}_4, \mathbf{Q}_f^t, \mathbf{Q}_{\text{box}}^t) \quad \mathbf{y}_t = \mathcal{C}(\mathbf{Q}_f^t) \quad \mathbf{b}_t = \mathbf{Q}_{\text{box}}^t, \quad (2)$$

producing segmentation masks  $\mathbf{M}_t$  and class probabilities

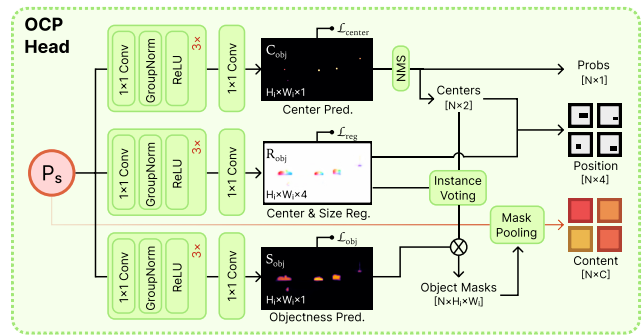


Figure 4. Architecture of the OCP module head.

$\mathbf{y}_t$  respectively. Bounding box predictions  $\mathbf{b}_t$  are obtained directly from  $\mathbf{Q}_{\text{box}}^t$ .

#### 3.1. Query initialization

Because of fundamental difference between the stuff and thing classes, we employ different strategies for the initialization (*i.e.*,  $\mathbf{Q}_f^0, \mathbf{Q}_{\text{box}}^0$ ) of each type. Stuff segmentation mainly requires learning different semantic concepts, which we capture using a set of  $N_{\text{st}}$  learnable queries [5]. In contrast, the detection of thing objects also requires the distinction between object instances, which has been shown to improve with the use of query selection (*i.e.* proposals) from image features [13]. To further addresses the scale imbalance of traditional query selection methods, and effectively capture both small and large objects, we introduce an Object-Centric Proposal extraction module (OCP) to extract  $N_{\text{th}}$  thing queries.

##### 3.1.1. Object-Centric Proposal Extraction (OCP)

In contrast to traditional pixel-level query selection mechanisms, OCP aims to extract proposals on a per-object level. To achieve this, OCP generates proposals by predicting an object center mask and using non-maxima suppression (NMS) to obtain object centers. On each of the feature

levels  $\mathbf{P}_s$ , an OCP head is built, as summarized in Figure 4. The OCP head is composed of three small predictions heads. The **center prediction head**, which serves as the proposal generator, outputs a center mask  $\mathbf{C}_{\text{obj}}$  with high activations at center locations of each object in the scene. The center locations  $x_i$  and their probabilities  $p_i$  are obtained by applying a NMS to  $\mathbf{C}_{\text{obj}}$ . Proposals are then ranked across all feature levels according to their probabilities  $p_i$  and the top  $N_{\text{th}}$  are selected for query extraction.

To extract positional query  $\mathbf{Q}_{\text{box}}^0(i)$  of object  $i$  we utilize a **regression head**, which predicts object center and size regression maps  $\mathbf{R}_{\text{obj}} \in \mathbb{R}^{H \times W \times 4}$ . Specifically, on each object pixel, a relative center location ( $\Delta x$ ,  $\Delta y$ ) and object bounding box size ( $w$ ,  $h$ ) are predicted. The positional queries of can be directly obtained from the regression values at the location  $x_i$ .

To extract the content query  $\mathbf{Q}_f^0(i)$ , the center location  $x_i$  might not be the most reliable. Instead, we rely on an approximate segmentation of the object that can be obtained from the regression maps  $\mathbf{R}_{\text{obj}}$  via instance voting. Each pixel is assigned to the proposal location  $x_i$  closest to it’s regressed center prediction. The approximate object mask  $\mathbf{m}_i$  for the object  $i$  at pixel  $j$  can be expressed as

$$m_i(j) = \begin{cases} 1, & \text{if } d_{i,j} = \min_k(d_{k,j}) \text{ and } d_{i,j} < \theta, \\ 0, & \text{otherwise.} \end{cases} \quad (3)$$

where  $d_{i,j}$  denotes the distance between a proposal location  $x_i$  and the regressed center location (from  $\mathbf{R}_{\text{obj}}$ ) at pixel  $j$ .  $\theta$  is a distance threshold – if no proposal locations are within  $\theta$  of the predicted center, the pixel is not assigned to any proposal.

Since the approximate masks are unreliable, in particular close to object edges, a third, **objectness head** classifies pixels into *thing objects* (1) vs. *stuff classes* (0), producing a binary segmentation mask  $\mathbf{S}_{\text{obj}}$ . To obtain the content query, we then use the probabilities in  $\mathbf{S}_{\text{obj}}$  for weighted mask pooling of image features  $\mathbf{P}_s$  inside  $m_i$

$$\mathbf{Q}_f^0(i) = \sum_j m_i(j) \mathbf{S}_{\text{obj}}(j) \cdot \mathbf{P}_s(j), \quad (4)$$

over all pixel locations  $j$ .

**Supervision.** Each OCP head is supervised independently via the following combination of losses

$$\mathcal{L}_{\text{OCP}}^s = \lambda_{\text{obj}} \mathcal{L}_{\text{obj}} + \lambda_{\text{reg}} \mathcal{L}_{\text{reg}} + \lambda_{\text{center}} \mathcal{L}_{\text{center}}. \quad (5)$$

The objectness head is supervised by a *pixel-wise focal loss*  $\mathcal{L}_{\text{obj}}$ , the regression head uses *L1 regressions loss*  $\mathcal{L}_{\text{reg}}$  based on ground-truth object bounding boxes, and the center prediction head uses *pixel-wise focal loss*  $\mathcal{L}_{\text{center}}$ , where the ground-truth center mask is constructed from small

isotropic gaussians at the object center location. Additionally, to enforce each feature pyramid level to focus on objects of a specific size range, we only supervise each level by objects within the level’s size range. Regions of the masks belonging to other objects are ignored in the loss computation for that level. More details about the OCP supervision are provided in the supplementary.

### 3.2. Object-Centric Mask Prediction

As is standard in mask transformer architectures [5], the mask predictions for each *stuff* query is obtained by correlating the respective query feature with the high-resolution image features  $\mathbf{P}_4$ . However, in the case of instance segmentation on the *thing* classes, such global similarity computation may be detrimental for separation of objects with similar appearance. Instead, we harness the positional information contained in the object positional queries  $\mathbf{Q}_{\text{box}}$ . Specifically, we limit the mask predictions of thing classes to the immediate area of the object region prescribed by the predicted bounding box  $\mathbf{Q}_{\text{box}}$ . At a pixel position  $x$ , the mask can be expressed as

$$\mathbf{M}_t(x) = \begin{cases} \sigma(\mathbf{P}_4(x) \cdot f(\mathbf{Q}_f)) & \text{if } x \text{ in } \phi(\mathbf{Q}_{\text{box}}, \epsilon_w, \epsilon_h), \\ 0 & \text{otherwise} \end{cases}, \quad (6)$$

where  $\sigma$  is the sigmoid activation function,  $f$  is a linear projection layer and  $\phi(\cdot, \epsilon_w, \epsilon_h)$  is a dilation function, that expands the bounding box both directions by a small margins defined by  $\epsilon_w$  and  $\epsilon_h$ . In other words, the mask probability outside the dilated bounding box is set to zero. The benefits of this approach are two-fold. First, the network avoids learning to separate objects at a global scale and can instead use it’s capacity to learn the separation of more challenging, overlapping instances in a local context. Second, this approach explicitly enforces consistency between object segmentation and bounding box prediction, reducing bounding-box-segmentation inconsistencies during matching and inference.

### 3.3. Training

Following the classic training procedure [13], we train PanSR by a combination of losses

$$\mathcal{L}_{\text{pred}} = \lambda_{\text{cls}} \mathcal{L}_{\text{cls}} + \lambda_{\text{mask}} \mathcal{L}_{\text{mask}} + \lambda_{\text{box}} \mathcal{L}_{\text{box}} \quad (7)$$

on matches between queries and ground-truth segments, where  $\mathcal{L}_{\text{cls}}$  is a binary sigmoid focal loss on predicted labels,  $\mathcal{L}_{\text{mask}}$  is a combination of sigmoid cross-entropy and DICE loss on predicted masks, and  $\mathcal{L}_{\text{box}}$  is a combination of L1 and generalized IoU losses on predicted bounding boxes. The total loss is a combination of the proposal and prediction losses

$$\mathcal{L} = \sum_s \mathcal{L}_{\text{OCP}}^s + \sum_t \mathcal{L}_{\text{pred}}^t, \quad (8)$$

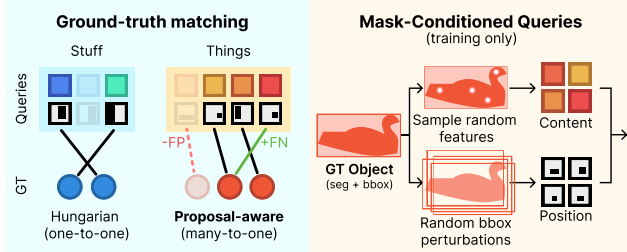


Figure 5. The proposal-aware matching scheme (left) alleviates the problem of false-negative and false-positive matches. Mask-conditioned queries (right) simulate random variation in content and positional queries of proposals during training.

where OCP is supervised at all feature levels  $s$  and predictions are supervised at the output every decoder layer  $t$ .

For supervising learnable *stuff* queries, we utilize standard Hungarian matching to compute maximal one-to-one matching between ground-truth and predictions. However, we observe such one-to-one matching approach is not ideal for queries constructed from proposals (*i.e.* *things*). For example, the proposal extractor may extract multiple queries for a single objects at different scales. In standard one-to-one matching only one of the queries is matched to the target object, while other queries are punished. Even worse, the unmatched proposals of one object may get matched to a different nearby object instead.

In theory, this should enable the decoder to utilize the redundant queries on one object to address neighboring objects with missing proposals instead. However, we observe in practice that such strategy leads to inconsistent decodings (*i.e.* query drift) from perfectly good query initializations, even when no alternative query proposals for that object exist (see Figure 2). Instead of relying on this inconsistent strategy, we propose an alternative proposal-aware matching scheme, where query decoding is encouraged to stay consistent with initial proposals.

### 3.3.1. Proposal-Aware Matching

The proposal-aware matching is posed as a refinement of a standard one-to-one matching. Specifically, we want to remove bad matches (false positives) and add high-quality alternative matches (false negatives) as demonstrated in Figure 5. First, maximal bipartite matching between GT and object queries is computed using the Hungarian algorithm, considering the predicted mask, bounding box and class label in the cost as in [13]. We then apply two refinement stages that address false-positive (FP) and false-negative (FN) matches respectively.

**Stage 1 – FP removal:** Missing proposals on a ground-truth object can lead to a forced matching to proposals from other objects. This stage aims to remove these bad matches.

Specifically, we remove matches with a low overlap of GT and predicted bounding box ( $\text{IoU} < \theta_{\text{FP}} = 0.25$ ). This prevents learning to move queries from one object to the other during decoding, addressing the query drift.

**Stage 2 – FN correction:** Due to the nature of multi-scale proposal extraction, multiple queries may be extracted for a single object, but bipartite matching will only select one, while others (FNs) will be diminished by the training. This stage aims to identify these alternative queries as unmatched queries with a significant overlap with a ground-truth object ( $\text{IoU} > \theta_{\text{FN}} = 0.80$ ), and add them as additional supervision matches.

Note that this stage largely removes the ability of the decoder to implicitly learn a NMS-like suppression between queries. At test-time we thus apply a classical NMS among detected bounding boxes, considering their predicted confidence scores [8, 15].

### 3.3.2. Mask-Conditioned Queries

The query proposal extraction (OCP from Section 3.1.1) is a noisy process. Thus, to make the decoder more robust to the noise in query extraction, we introduce a set of additional randomized mask-conditioned queries during training akin to de-noising approaches [12, 13]. Mask-conditioned queries are simulated by sampling features at random scales and from random locations inside the ground-truth object masks.

In contrast to existing de-noising strategies, which obtain features by perturbing a learned class embedding, this approach more closely simulates test-time proposal extraction process. To initialize the positional query (bounding box) we use perturbed ground-truth bounding boxes as in [12]. Each of these queries are matched and supervised with their respective ground-truth object. The mask-conditioned queries only interact with each other in the decoder and not with regular queries.

## 4. Experiments

We compare PanSR with state-of-the-art methods on LaRS (Section 4.2), a challenging recent panoptic maritime benchmark, and on Cityscapes (Section 4.3). A detailed ablation study of PanSR is then reported in Section 4.4.

### 4.1. Implementation details

The architecture of the transformer encoder and decoder follows [13]. We set the number of learnable stuff queries  $N_{\text{st}} = 50$ , thing queries  $N_{\text{th}} = 250$  and mask-conditioned queries  $N_{\text{dn}} = 100$ . We set  $\theta = 0.02 \cdot w$ , where  $w$  is the feature-map width at that level. For bounding-box dilation during mask prediction we use  $\epsilon_w = \min(0.1 \cdot w, 2)$ ,  $\epsilon_h = \min(0.1 \cdot h, 2)$  pixels, where  $(w, h)$  is the size of the bounding box in pixels. We use  $L = 9$  layers in the transformer

	Method	Backbone	PQ (%)				RQ (%)				SQ (%)			
			All	Th	Th <sub>a</sub>	St	All	Th	Th <sub>a</sub>	St	All	Th	Th <sub>a</sub>	St
Single-stage	Panoptic Deeplab [3]	ResNet-50	34.7	13.4	33.0	91.4	40.3	19.3	46.3	96.2	69.5	60.0	71.3	94.9
	Panoptic FPN [10]	ResNet-50	40.1	21.7	35.5	89.3	46.9	28.6	45.9	95.8	73.5	66.1	77.3	93.1
		ResNet-101	38.7	19.7	35.5	89.4	45.0	26.1	46.0	95.5	73.6	66.1	77.1	93.5
	Mask2Former [5]	ResNet-50	37.6	17.0	27.9	92.4	43.7	23.6	37.6	97.3	71.3	62.4	74.2	95.0
		Swin-B	41.7	21.8	33.6	94.7	48.5	29.7	44.6	98.5	78.2	71.5	75.3	96.2
	MaX-DeepLab [16]	MaX-S	31.9	9.5	19.2	91.7	36.1	13.4	26.0	96.6	71.3	62.5	73.7	94.8
	Mask DINO (1S) [13]	ResNet-50	41.4	22.3	30.0	92.5	47.1	28.9	37.9	95.8	75.2	67.2	79.2	96.5
OneFormer [9]	Swin-L	35.2	12.8	27.8	95.0	39.2	17.1	36.6	98.2	74.3	65.8	76.0	96.7	
Two-stage	Mask DINO (2S) [13]	ResNet-50	50.1	34.2	47.7	92.5	59.0	45.0	61.4	96.1	74.5	66.3	77.8	96.2
		Swin-L	53.9	38.9	54.6	93.8	63.0	50.1	69.3	97.1	75.6	67.7	78.8	96.5
	PanSR	ResNet-50	54.2	39.3	56.3	94.1	63.9	51.1	71.6	97.8	82.6	77.4	78.6	96.2
		Swin-L	57.3	43.0	60.4	95.4	66.9	55.0	75.8	98.7	75.9	68.2	79.7	96.7

Table 1. Panoptic segmentation on the LaRS test set. Top three results for each metric are outlined in gold, silver and bronze.

decoder. Unless explicitly stated otherwise, we utilize a ResNet-50 backbone in all our experiments and visualizations.

We adopt the training strategy (losses, LR scheduling, optimizer) from [13]. We set the loss weights  $\lambda_{\text{obj}} = \lambda_{\text{reg}} = \lambda_{\text{center}} = 5$  and  $\lambda_{\text{cls}} = 4$ ,  $\lambda_{\text{mask}} = \lambda_{\text{box}} = 5$ . For experiments on LaRS, we train PanSR on  $4 \times$  A100 GPUs with a total batch size of 8 images for 90k training iterations. We apply the same training schedule to baseline methods.

The copy-paste augmentation [7] is used in training, pasting additional thing objects from the dataset at random locations in the image. For LaRS, we paste objects inside the water region. We adopt an identical training strategy for Cityscapes, with the exception of using  $8 \times$  A100 GPUs with a total batch size of 16 images. We do not employ copy-paste augmentations during training on Cityscapes.

## 4.2. Panoptic segmentation on LaRS

LaRS [24] is a maritime, panoptic, scene-understanding benchmark for autonomous surface vessels. It contains over 4000 visually diverse aquatic scenes split into training, validation and a sequestered test sets. Scenes are labeled with per-pixel panoptic annotations for 4 stuff classes and 8 thing (obstacles) classes with over 21,000 thing objects. A wide range of object sizes and crowded scenes are some of the key challenges of LaRS. We follow a standard evaluation protocol, reporting Panoptic Quality (PQ) [11] on the LaRS test set through the evaluation server [24]. PQ combines the measure for instance recognition quality (RQ), and the measure of segmentation quality (SQ). Class-averaged (All) results are reported, as well as scores on thing (Th) and stuff (St) classes separately. In addition, LaRS also measures class-agnostic performance for thing classes (Th<sub>a</sub>), where all thing objects are treated as a single class.

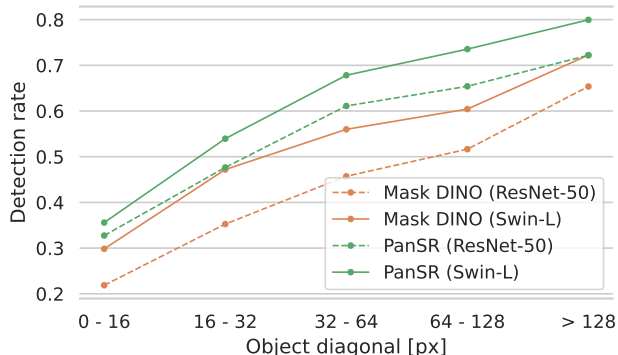


Figure 6. Object detection rate w.r.t. object size.

PanSR is compared with the recent state-of-the-art mask transformer methods Mask2Former [5], MaX-DeepLab [16], Mask DINO [13], OneFormer [9], and with established convolutional methods Panoptic Deeplab [3] and Panoptic FPN [10].

The results are shown in Table 1. Both Mask DINO and PanSR outperform all single-stage methods by a large margin, which demonstrates the importance of query selection for this task. Among the two-stage methods, PanSR achieves a new state-of-the-art by +3.4% PQ over Mask DINO with Swin-L backbone. Interestingly, PanSR w/ ResNet-50 matches the performance Mask DINO w/ Swin-L, despite a significantly lower backbone complexity, highlighting the effectiveness of its design.

Remarkable improvements of PanSR are observed in detection robustness, reflected in the recognition quality metric (RQ). In the thing-classes detection, PanSR outperforms the second-best method by nearly 5%. This is further confirmed by the qualitative analysis (Figure 7), which reveals that PanSR largely eliminates instance grouping of similar objects, facilitating superior detection performance. Com-

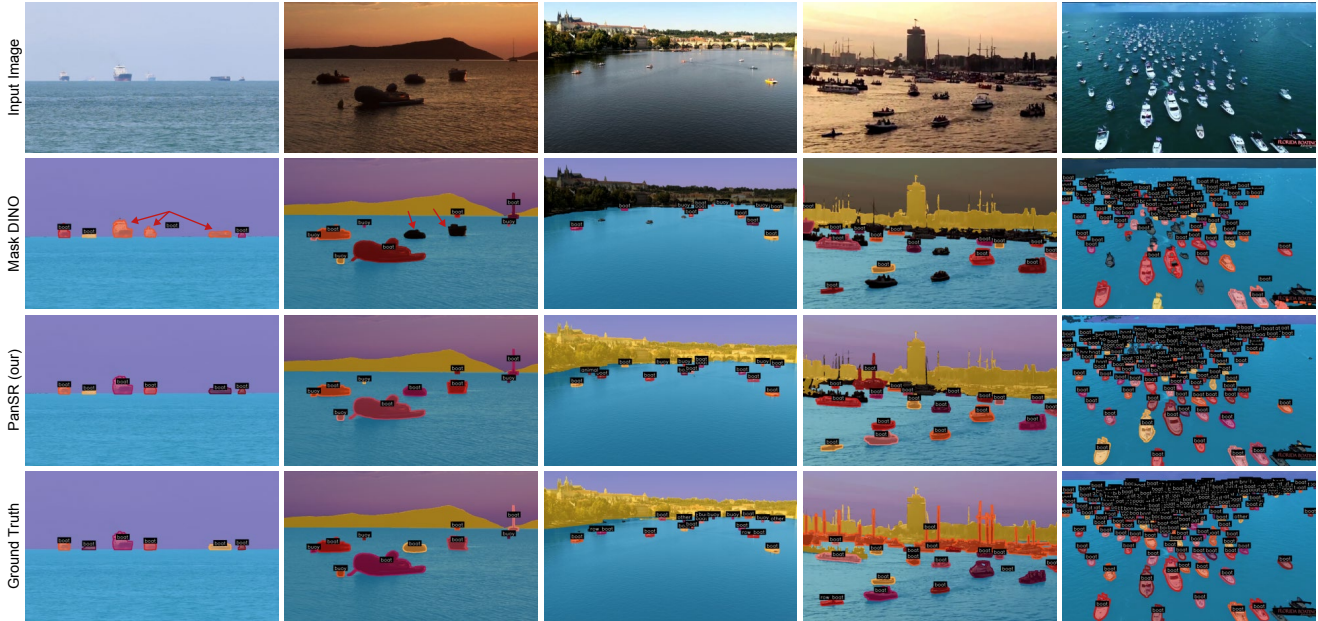


Figure 7. Qualitative results on LaRS. Addressing instance merging (col. 1, 2 & 4), small objects (col. 3 & 5) and crowded scenes (col. 5).

pared to other methods, PanSR is also much more accurate in the detection of small objects as shown in Figure 7. Additional analysis of detection rate across different object scales, visualized in Figure 6, demonstrates that PanSR significantly improves the performance across all instance sizes.

### 4.3. Panoptic segmentation on Cityscapes

We compare PanSR with the state-of-the-art panoptic segmentation methods on Cityscapes [6], featuring urban driving scenes. As is common practice, we train PanSR on the training set and report the performance on the val split measured by PQ for panoptic performance, average precision (AP) for detection performance on the thing classes, and mean IoU for semantic segmentation performance.

PanSR is compared with the recent state-of-the-art mask transformer methods Mask2Former [5] and OneFormer [9], as well as established convolutional methods Panoptic Deeplab [3], Panoptic FPN [10] and Axial-DeepLab [17]. For fair comparison, we include only methods trained exclusively on Cityscapes. The results are shown in Table 2. Using the same parameters as in LaRS and without dataset-specific hyperparameter optimization, PanSR reaches a competitive performance among the state-of-the-art methods with a PQ of 67.2, on par with the best method OneFormer [9].

Note that OneFormer has been trained in a multi-task setup, optimizing for panoptic, instance and semantic segmentation jointly and thus enjoys increased performance on the instance (AP) and segmentation (mIoU) tasks. Qualitative results (Figure 9) confirm that PanSR effectively ad-

Method	Backbone	PQ	AP	mIoU
Panoptic-DeepLab	ResNet-50	59.7	-	-
	Xception-71	63.0	35.3	80.5
Panoptic FPN	ResNet-50	57.7	32.0	75.0
Axial-DeepLab	Axial ResNet-L	63.9	35.8	81.0
	Axial ResNet-XL	64.4	36.7	80.6
Mask2Former	ResNet-50	62.1	37.3	77.5
	Swin-L	66.6	43.6	82.9
OneFormer	Swin-L	67.2	45.6	84.4
PanSR	ResNet-50	62.4	37.1	77.3
	Swin-L	67.2	43.5	82.9

Table 2. Panoptic segmentation results on Cityscapes val.

resses instance merging issues. Furthermore, PanSR substantially outperforms OneFormer (by +22.1 PQ) on LaRS, confirming its excellent generalization capabilities.

### 4.4. Ablation study

We ablate the major contributions of PanSR on the LaRS test set. Results are shown in Table 3. We first investigate the impact of the proposed OCP module (Section 3.1.1) for query selection. Using only learnable queries results in a substantial performance drop on foreground classes. Using the classical query selection mechanisms [13] dramatically improves performance (+5.7% PQ). Separation into learnable queries for stuff and proposals for thing classes [21] (denoted “*Lrn.* + *QS*”) additionally improves performance. Finally, replacing the classical query selection with the pro-

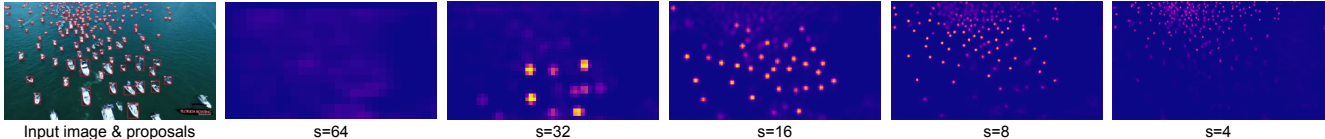


Figure 8. Object center predictions of the OCP module. Each OCP level (denoted by stride  $s$ ) is specialized for objects of specific sizes.

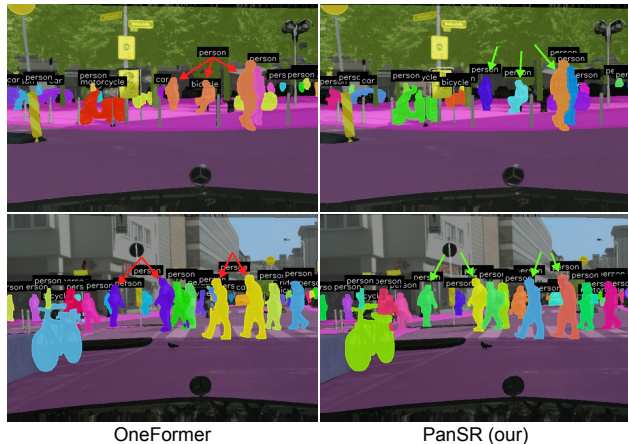


Figure 9. Qualitative comparison on Cityscapes val. OneFormer (left) incorrectly merges spatially well-separated instances, while PanSR (right) correctly resolves them.

Component	Variant	PQ	PQ <sub>th</sub>	aPQ <sub>th</sub>
Queries	Learnable [5]	43.3	24.4	36.7
	Query Selection [13]	49.0	33.8	49.1
	Lrn. + QS [21]	51.8	36.0	52.5
	<b>Lrn. + OCP</b>	<b>54.2</b>	<b>39.3</b>	<b>56.3</b>
Mask	Global	52.0	36.2	51.9
	Strict BBox	50.2	33.8	52.0
	<b>Relaxed BBox</b>	<b>54.2</b>	<b>39.3</b>	<b>56.3</b>
Matching	Hungarian [2]	53.3	38.2	54.4
	<b>Proposal-aware</b>	<b>54.2</b>	<b>39.3</b>	<b>56.3</b>
Conditioned Queries	No	53.1	37.8	55.9
	DN-DETR [12]	53.9	38.9	56.2
	<b>Mask-conditioned</b>	<b>54.2</b>	<b>39.3</b>	<b>56.3</b>

Table 3. Ablations of various components of PanSR on LaRS test set, measured in PQ, PQ<sub>th</sub> on thing classes and class-agnostic aPQ<sub>th</sub>.

posed OCP module (“Lrn. + OCP”) leads to a large PQ improvement of 2.4%. The difference is especially apparent on the thing classes (+3.4 PQ<sub>th</sub>). Figure 8 illustrates how the OCP head’s center predictions accurately target objects across varying scales.

Next, we analyze the importance of object-centric mask prediction (Section 3.2). Traditional global mask predictions hinder the performance on thing classes. Applying strict bounding-box constraints to masks of foreground

classes is also suboptimal and, in fact, reduces the performance by 1.8%, as tight bounding boxes interfere with the segmentation of the object. Relaxing these constraints via the proposed bounding box dilation allows additional breathing room for the segmentation, while still constraining it to the immediate area of the object, and results in +2.2% PQ over global segmentation. The effectiveness of this approach is also evidenced qualitatively by a substantial reduction in instance merging issues as shown in Figure 7.

We also investigate our proposal-aware matching scheme (Section 3.3.1) for thing classes and compare it to traditional one-to-one Hungarian matching. Proposal-aware matching boosts PQ by 0.9% compared to the traditional approach. Finally, we consider the impact of mask-conditioned queries during training. In comparison to de-noising approaches [12], the mask-conditioned queries of PanSR improve performance by 0.3% PQ.

## 5. Conclusion

We presented PanSR, a novel mask-transformer approach for panoptic segmentation, that addresses key issues of existing approaches such as scale imbalance in query selection, instance merging among visually similar objects, and query drift from good initialization. PanSR achieves this by applying an object-centric approach to proposal generation, mask prediction and ground-truth matching.

Extensive evaluation of PanSR on the challenging LaRS benchmark, featuring a large diversity of different object scales, crowded scenes and small objects, reveals superior performance across all object sizes and eliminates most cases of instance merging as outlined by our qualitative analysis. PanSR also performs on par with state-of-the-art performance among comparable methods on heavily optimized Cityscapes benchmark, without any additional hyperparameter tuning, demonstrating its good generalization capabilities. By addressing key challenges in scale-robust object detection and instance separation, PanSR brings panoptic segmentation closer to practical use in both autonomous maritime and ground vehicles.

The main contributions of PanSR are complementary to other recent directions in panoptic segmentation such as language-based open-vocabulary [21] mask classification and multi-task learning [9]. We will explore these avenues in our future work.



## Acknowledgements.

This work was supported by Slovenian research agency program P2-0214 and project J2-2506, and by a supercomputing network SLING (ARNES, EuroHPC Vega - IZUM).

## References

- [1] Holger Caesar, Jasper Uijlings, and Vittorio Ferrari. COCO-Stuff: Thing and Stuff Classes in Context. *CVPR*, pages 1209–1218, 2016. 1
- [2] Nicolas Carion, Francisco Massa, Gabriel Synnaeve, Nicolas Usunier, Alexander Kirillov, and Sergey Zagoruyko. End-to-End Object Detection with Transformers. *Lecture Notes in Computer Science (including subseries Lecture Notes in Artificial Intelligence and Lecture Notes in Bioinformatics)*, 12346 LNCS:213–229, 2020. 2, 8
- [3] Bowen Cheng, Maxwell D Collins, Yukun Zhu, Ting Liu, Thomas S Huang, Hartwig Adam, and Liang-Chieh Chen. Panoptic-DeepLab: A Simple, Strong, and Fast Baseline for Bottom-Up Panoptic Segmentation. In *Proceedings of the IEEE/CVF Conference on Computer Vision and Pattern Recognition (CVPR)*, pages 12475–12485, 2020. 2, 6, 7
- [4] Bowen Cheng, Alexander G. Schwing, and Alexander Kirillov. Per-Pixel Classification is Not All You Need for Semantic Segmentation. *Advances in Neural Information Processing Systems*, 34, 2021. 1, 2
- [5] Bowen Cheng, Ishan Misra, Alexander G. Schwing, Alexander Kirillov, and Rohit Girdhar. Masked-attention Mask Transformer for Universal Image Segmentation. In *2022 IEEE/CVF Conference on Computer Vision and Pattern Recognition (CVPR)*, pages 1280–1289, 2022. 1, 2, 3, 4, 6, 7, 8
- [6] Marius Cordts, Mohamed Omran, Sebastian Ramos, Timo Rehfeld, Markus Enzweiler, Rodrigo Benenson, Uwe Franke, Stefan Roth, and Bernt Schiele. The Cityscapes Dataset for Semantic Urban Scene Understanding. In *Proceedings of the IEEE Conference on Computer Vision and Pattern Recognition (CVPR)*, 2016. 1, 2, 7
- [7] Golnaz Ghiasi, Yin Cui, Aravind Srinivas, Rui Qian, Tsung-Yi Lin, Ekin D. Cubuk, Quoc V. Le, and Barret Zoph. Simple Copy-Paste is a Strong Data Augmentation Method for Instance Segmentation. In *2021 IEEE/CVF Conference on Computer Vision and Pattern Recognition (CVPR)*, pages 2917–2927, 2021. 6
- [8] Kaiming He, Georgia Gkioxari, Piotr Dollár, and Ross Girshick. Mask R-CNN. In *2017 IEEE International Conference on Computer Vision (ICCV)*, pages 2980–2988, 2017. 5
- [9] Jitesh Jain, Jiachen Li, MangTik Chiu, Ali Hassani, Nikita Orlov, and Humphrey Shi. OneFormer: One Transformer to Rule Universal Image Segmentation. In *Proceedings of the IEEE/CVF Conference on Computer Vision and Pattern Recognition*. arXiv, 2023. 1, 2, 6, 7, 8
- [10] Alexander Kirillov, Ross Girshick, Kaiming He, and Piotr Dollár. Panoptic Feature Pyramid Networks. In *Proceedings of the IEEE/CVF Conference on Computer Vision and Pattern Recognition (CVPR)*, pages 6399–6408, 2019. 2, 6, 7
- [11] Alexander Kirillov, Kaiming He, Ross Girshick, Carsten Rother, and Piotr Dollár. Panoptic segmentation. In *Proceedings of the IEEE Computer Society Conference on Computer Vision and Pattern Recognition*, pages 9396–9405. IEEE Computer Society, 2019. 2, 6
- [12] Feng Li, Hao Zhang, Shilong Liu, Jian Guo, Lionel M. Ni, and Lei Zhang. DN-DETR: Accelerate DETR Training by Introducing Query DeNoising. In *Proceedings of the IEEE/CVF Conference on Computer Vision and Pattern Recognition*, pages 13619–13627, 2022. 2, 5, 8
- [13] Feng Li, Hao Zhang, Huaizhe xu, Shilong Liu, Lei Zhang, Lionel M. Ni, and Heung-Yeung Shum. Mask DINO: Towards A Unified Transformer-based Framework for Object Detection and Segmentation, 2022. 1, 2, 3, 4, 5, 6, 7, 8
- [14] Shilong Liu, Feng Li, Hao Zhang, Xiao Yang, Xianbiao Qi, Hang Su, Jun Zhu, and Lei Zhang. DAB-DETR: Dynamic Anchor Boxes are Better Queries for DETR. In *International Conference on Learning Representations*, 2021. 2
- [15] Jer Pelhan, Alan Lukežič, Vitjan Zavrtanik, and Matej Kristan. DAVE – A Detect-and-Verify Paradigm for Low-Shot Counting. *2024 IEEE/CVF Conference on Computer Vision and Pattern Recognition (CVPR)*, pages 23293–23302, 2024. 5
- [16] Huiyu Wang, Yukun Zhu, Hartwig Adam, Alan Yuille, and Liang-Chieh Chen. MaX-DeepLab: End-to-End Panoptic Segmentation with Mask Transformers. In *Proceedings of the IEEE/CVF Conference on Computer Vision and Pattern Recognition (CVPR)*, pages 5463–5474, 2020. 2, 6
- [17] Huiyu Wang, Yukun Zhu, Bradley Green, Hartwig Adam, Alan L. Yuille, and Liang-Chieh Chen. Axial-DeepLab: Stand-Alone Axial-Attention for Panoptic Segmentation. In *European Conference on Computer Vision*, pages 108–126, 2020. 7
- [18] Yuwen Xiong, Renjie Liao, Hengshuang Zhao, Rui Hu, Min Bai, Ersin Yumer, and Raquel Urtasun. Upsnet: A unified panoptic segmentation network. In *Proceedings of the IEEE/CVF Conference on Computer Vision and Pattern Recognition (CVPR)*, 2019. 2
- [19] Jiarui Xu, Sifei Liu, Arash Vahdat, Wonmin Byeon, Xiaolong Wang, and Shalini De Mello. Open-Vocabulary Panoptic Segmentation with Text-to-Image Diffusion Models, 2023. 2
- [20] Hao Zhang, Feng Li, Shilong Liu, Lei Zhang, Hang Su, Jun Zhu, Lionel M. Ni, and Heung-Yeung Shum. DINO: DETR with Improved DeNoising Anchor Boxes for End-to-End Object Detection, 2022. 2
- [21] Hao Zhang, Feng Li, Xueyan Zou, Shilong Liu, Chunyuan Li, Jianfeng Gao, Jianwei Yang, and Lei Zhang. A Simple Framework for Open-Vocabulary Segmentation and Detection, 2023. 1, 2, 7, 8
- [22] Bolei Zhou, Hang Zhao, Xavier Puig, Tete Xiao, Sanja Fidler, Adela Barriuso, and Antonio Torralba. Semantic Understanding of Scenes Through the ADE20K Dataset. *Int J Comput Vis*, 127(3):302–321, 2019. 1
- [23] Xizhou Zhu, Weijie Su, Lewei Lu, Bin Li, Xiaogang Wang, Jifeng Dai, and Sensetime Research. Deformable DETR:

Deformable Transformers for End-to-End Object Detection. 2020. [2](#)

- [24] Lojze Žust, Janez Perš, and Matej Kristan. LaRS: A Diverse Panoptic Maritime Obstacle Detection Dataset and Benchmark. In *Proceedings of the IEEE/CVF International Conference on Computer Vision*, pages 20304–20314, 2023. [1](#), [2](#), [6](#)

# PanSR: An Object-Centric Mask Transformer for Panoptic Segmentation

## Supplementary Material

### 6. OCP supervision details

#### 6.1. Center prediction ground truth

To construct the ground-truth center masks  $\hat{C}_{\text{obj}}$  for supervision of the *center prediction head* (see Section 3.1.1), we utilize the following procedure. First, an object center  $\mathbf{c}_i = (c_x, c_y)$  is extracted from each object’s bounding box. A small isotropic 2D Gaussian is then constructed at the object center location. Specifically, the center mask  $\hat{C}_{\text{obj}}^i$  of object  $i$  is computed as

$$\hat{C}_{\text{obj}}^i(\mathbf{x}) = \exp\left(-\frac{1}{2} \frac{\|\mathbf{x} - \mathbf{c}_i\|^2}{\sigma^2}\right), \quad (9)$$

where  $\mathbf{x} = (x_x, x_y)$  is a pixel location in the mask and  $\sigma^2 = 1\text{px}$  is the variance of the Gaussian function. The same fixed variance is used to construct object masks at all OCP levels. Gaussians for individual objects are combined in the final ground-truth center mask using a maximum operation

$$\hat{C}_{\text{obj}}(\mathbf{x}) = \max_i \left( \hat{C}_{\text{obj}}^i(\mathbf{x}) \right). \quad (10)$$

Examples of center predictions obtained using such supervision are shown in Figure 8 of the main paper.

#### 6.2. Targeting specific object sizes

To ensure balance between object scales, each OCP head (Section 3.1.1) specializes in objects of specific scale. We measure the object scale as the bounding box diagonal  $d$  (in pixels of the original image). The scale ranges of each OCP level are presented in Table 4. There is a slight overlap between objects targeted by neighboring levels, to ensure consistent operation for objects whose size is close to the limit of each level.

We wish to extract proposals only for objects within the size range of the current level, thus *center mask prediction* at all other object center locations are supervised as 0. On the other hand, for the predictions of the *regression* and the *objectness* heads, we relax the supervision slightly. Instead of forcing zero-outputs on objects not in the scale range, we ignore their contributions to the loss instead. This way, the heads may learn the simplest strategy for predicting regression and objectness outputs at that scale, without the need to differentiate between objects of different scales.

### 7. Additional qualitative examples

In Figures 10 and 11 we present additional qualitative results of PanSR and state-of-the-art methods Mask DINO [13] and OneFormer[9] on the LaRS test set and Cityscapes val set respectively.

OCP level	size range ( $d$ )
$s = 64$	$[256, \infty]$
$s = 32$	$[128, 512]$
$s = 16$	$[64, 256]$
$s = 8$	$[32, 128]$
$s = 4$	$[0, 64]$

Table 4. Size ranges of objects, that are used for supervision at different OCP levels.



Figure 10. Additional qualitative examples on the LaRS test set.

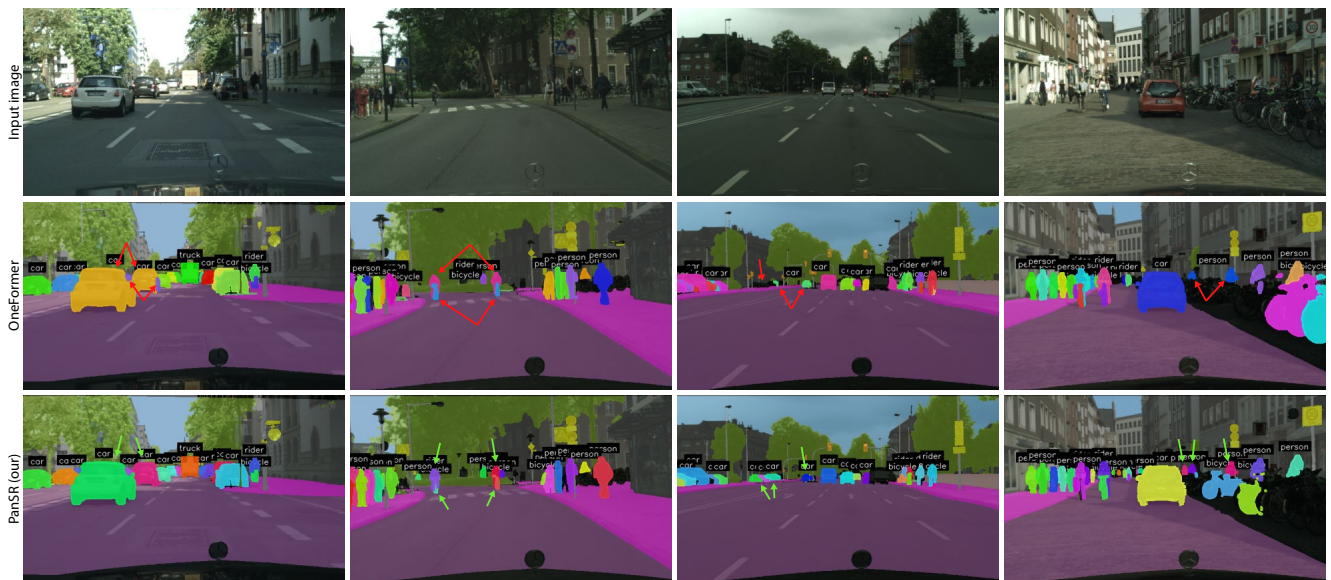


Figure 11. Additional qualitative examples on the Cityscapes val set.